

Chemical characterization and nanomechanical properties of antiwear films fabricated from ZDDP on a near hypereutectic Al–Si alloy

G. Pereira^a, A. Lachenwitzer^a, M.A. Nicholls^a, M. Kasrai^a, P.R. Norton^{a,*} and G. De Stasio^b

^aDepartment of Chemistry, University of Western Ontario, London, Ontario, Canada N6A 5B7

^bPhysics Department, University of Wisconsin at Madison, Madison, WI, USA 53706

Received 9 August 2004; accepted 29 November 2004

X-ray absorption near edge structure (XANES) spectroscopy was used to monitor the products formed during the breakdown of the engine additive ZDDP during its action as a protective tribochemical agent. This investigation examines the film formed under various physical conditions on a near hypereutectic Al–Si alloy. For the first time, tribochemical films (tribofilms) formed on a high silicon weight content alloy, with virtually no ferrous component have been studied. Phosphorus K- and L-edge spectroscopies show that under typical engine operating conditions, the tribofilms have similar chemical composition over a range of different test conditions. X-ray photoelectron emission microscopy (X-PEEM) reveals that the polyphosphate glasses formed vary in chain length within localized regions. The mechanical properties of the substrate and the tribofilms were acquired using a Triboscope[®] from Hysitron Inc. The elastic moduli can be extracted from the indentation curves and show that the tribofilms' mechanical properties are similar to those of the tribofilms which form on steel under similar conditions.

KEY WORDS: ZDDP, XANES, X-PEEM, nanoindentation, polyphosphate, mechanical properties, tribofilm

1. Introduction

Due to the continuous effort in the automobile industry to reduce costs, to improve car design, and to increase fuel economy, there is a considerable incentive to reduce or replace the cast iron content in engines in order to reduce weight and frictional forces between surfaces which ultimately leads to wear.

Aluminum itself is a poor alternative to replace steel due to its inadequate wear resistance, and thus aluminum alloys have been introduced, that offer better wear protection, higher strength and fracture toughness, high specific rigidity, good thermal and electrical conductivity, and easy machining [1]. Alloying aluminum with silicon can increase the strength of aluminum as it is known to form a separate hard phase in an aluminum matrix.

One such alloy that has been developed and is currently used by DaimlerChryslerTM is manufactured by PEAK Werkstoff GmbHTM and is marketed under the name Silitec 5TM. This alloy is currently used in many vehicles as a cylinder sleeve. It is prepared by a spray-compaction method (Osprey process) [2] which generates a high silicon weight content (23–26 wt.%) [1,3] alloy, in which the silicon grains resemble a hypereutectic two phase microstructure [4–6]. This process leads to very small silicon grain size with a narrow distribution. The walls of the cylinder liner are chemically etched to expose the primary silicon grains on the sur-

face, ideally to provide a load bearing surface [1,3]. Other advantages of the Silitec 5TM alloy over conventional die cast two phase alloys includes easier machinability, and etching this near hypereutectic alloy with such a unique microstructure is a very small but uniformly distributed volume, which provides a reservoir for oil retention thus reducing the amount of oil consumed by around 30% [3].

The lubrication demands are expected to be different for steel and aluminum alloys as the microstructure and chemical properties are not similar. A great deal of research has been carried out on the dry-sliding wear response of many Al–Si alloys [7–13], however little research has been carried out on the lubrication of these alloys. Currently, the most important antiwear and antioxidant additive that is added to engine oils is a class of molecules called zinc dialkyl dithiophosphates (ZDDPs) [14]. Antiwear films generated from ZDDPs are known to protect rubbing surfaces in engines, acting as sacrificial films when being rubbed that are constantly regenerated in a rubbing environment [15]. Studies have shown that the breakdown products of ZDDPs, and not the ZDDPs itself, provides the antiwear protection needed to lubricate sliding steel surfaces within a simulated and actual engine environment [16,17]. Several studies show that ZDDPs decomposes upon rubbing to form a protective film (tribofilm or antiwear film), however thermal decomposition has also been the accepted major mechanism of the antiwear film formation [18–20]. It is well known that these films are comprised of an amorphous polyphosphate glass structure

*To whom correspondence should be addressed.
E-mail: pnorton@uwo.ca

[18,21–24]. The mechanism for antiwear film formation has been proposed [18,21], however these studies, using X-ray absorption near-edge structure (XANES) from a synchrotron source, have been thus far conducted on steel. This is the first characterization of tribofilms formed on the Silitec 5TM alloy with virtually no iron content.

XANES is a very good technique for acquiring detailed spatially averaged chemical information pertaining to a material or a thin film. However, for sub-micron local resolution of a specific species, X-ray photoelectron emission microscopy (X-PEEM) has made great advances with the advent of synchrotron radiation [25–28]. Recently, X-PEEM has been carried out on chosen features of the antiwear film formed from ZDDP on steel [24,29], and on a ferrous Al–Si alloy, A390 (16–18% Si, ~1.3% Fe) [30].

Morphological and topographical surface characterization plays an essential role in examining the antiwear films formed, which has been the subject of numerous studies [24,31–36]. The thickness of the tribofilms has been described as a key attribute for the antiwear performance, as the film acts as a sacrificial layer and minimizing the asperity contact between surfaces [36].

The mechanical properties of the antiwear pads have also been the subject of numerous studies [24,30,31,36,37], as it is believed that the mechanical response of these films are the primary reason for the antiwear performance. The indentation modulus values have been acquired through nanoindentation. The indentation modulus found on antiwear pads formed on Si from the A390 alloy was $\sim 76 \pm 7$ GPa [30].

In this paper, a spatial chemomechanical analysis of the antiwear films formed on the Silitec 5TM alloy was performed. Many variables that mimic operating conditions in an automobile engine were compared. The antiwear films that are formed were examined using XANES spectroscopy and X-PEEM to gain chemical information. Atomic force microscopy (AFM) and scanning electron microscopy (SEM) were used to gather topographical and morphological insight, while imaging nanoindentation was performed to acquire the mechanical properties of these films.

2. Experimental

2.1. Sample preparation

The aluminum-based Silitec 5TM alloy (~25% Si, ~4% Cu, ~1% Mg, <0.3% Fe) was machined into disks with dimensions of 17 mm \pm 0.5 mm radius and 3.5 \pm 0.5 mm thickness. The disks were mechanically polished using 0.3 μ m, 0.06 μ m alumina slurry suspensions and finally using a 0.03 μ m alumina paste. A weak caustic etching step using 5% NaOH was applied, which selectively dissolved away the aluminum matrix, at room temperature. This alloy is etched for commercial use so

that the embedded silicon grains stand proud of the aluminum rich matrix [1].

Commercial ZDDP consisting of secondary butyl groups (85%) and *n*-octyl groups (15%) in MCT-10 base oil was obtained from Imperial Oil (Esso) of Canada. ZDDP solutions were prepared by mixing ZDDP concentrate in MCT-10 base oil.

Antiwear films were made on the Silitec 5TM alloy disk using steel pins in a Plint high frequency wear tester. The Silitec 5TM disks and cylindrical 52100 steel pins were cleaned in an ultrasonic bath using a light hydrocarbon solvent, and then placed in the Plint high frequency wear tester. The ZDDP solution was placed in the Plint wear tester and the steel pin was laid flat against the disk (cylindrical face in contact with the surface). The frequency used to generate the tribofilms was maintained at 25 Hz. The influence of various experimental parameters was studied independently changing one variable at one time, versus the standard conditions (see table 1). Parameters such as etching time of the substrate, rubbing time, temperature, ZDDP concentration, and applied load were tested. After each experiment, excess oil was removed from the disks using tissue paper and then the samples were rinsed in hexane.

A grid consisting of indented marks was created using a Vickers hardness tester using loads of 100 and 500 g which made indents ~ 25 μ m and ~ 100 μ m across respectively. The grid allowed for relocation of the same region with multiple techniques. The wear tests were made in duplicate.

2.2. Morphology and topography data acquisition

AFM topography images were compiled for all the samples in air using a Nanoscope IIIa equipped with a MultimodeTM head (Digital Instruments, Santa Barbara, CA). The images were collected in contact force mode with a V-shaped silicon nitride cantilever possessing a spring constant of 0.12 N/m.

The SEM data were collected using a Hitachi S4500 SEM equipped with an EDAXTM light element EDX microanalysis system. Images were acquired with a 5 kV acceleration electron beam voltage, 17 mm working distance, and 30° tilt in the field emission mode.

Table 1.
Variations in the physical parameters studied.

Experimental parameters	Conditions
Etching time of the substrate (s)	15, 30, 45
Rubbing time (min)	5, 30, 180, 720
Temperature (°C)	100, 150, 200
Applied force (N)	100, 150, 200
ZDDP concentration (wt.%) in MCT-10 base oil	0.3, 0.6, 0.8, 1.2
Standard conditions	30 s etched substrate, 30 min, 100 °C, 100 N, 1.2% ZDDP solution

2.3. XANES spectroscopy and X-PEEM spectromicroscopy data acquisition

XANES data were obtained at the Canadian Synchrotron Radiation Facility (CSRF) [38], situated at the 1 GeV Aladdin storage ring, University of Wisconsin, Madison. Phosphorus, sulphur and silicon K-edge spectra were obtained on the double-crystal monochromator (DCM) [39] covering an energy range of 1500–4000 eV with photon resolution of 0.8 eV. Phosphorus, sulphur and silicon L-edge spectra were obtained on the Grasshopper soft X-ray beamline covering an energy range of 70–900 eV with photon resolution of 0.2 eV at the phosphorus L-edge. The energy scales for the phosphorus K- and L-edges were calibrated using pure ZDDP. The energy scale for sulphur K- and L-edges was calibrated using ZnS and FeS₂. The analyzed area was about 2 mm × 2 mm. The photoabsorption spectra for both the model compounds and samples were recorded in the total electron yield (TEY) mode and fluorescence yield (FY) mode for both surface and bulk sensitivity [40]. All spectra shown in this paper are an average of three scans that were digitally combined and normalized, with a linear background subtracted using the BAN program [41]. The assignment of the fine structure in XANES was carried out using model compounds obtained by the authors or by comparison to previous results.

Peak fitting was performed to provide semi-quantitative results for the amount of each, phosphorus and sulphur species, present in the wear scar. Phosphorus and sulphur K- and L-edge spectra were fitted using the BGAUSS program [42]. Peaks were fitted using a Voigt line (80% Lorentz, 20% Gaussian) and specific constraints to the elements absorption edge, similar to previous efforts [43]. An arctangent step function representing the transition of ejected photoelectrons to the continuum has been fitted to the spectra. The peak widths and positions for the spin-orbit splitting were fixed to be equal. The decay of the arctangent was also fixed for each fit. All other parameters were allowed to vary. In some instances, the Voigt peaks representative of the phosphorus and sulphur species were fixed to specific energy positions close to what was expected for the particular species. The relative fraction of each species was calculated by determining the area of the Voigt peak for that species divided by the total area of all the Voigt peaks for each phosphorus species present in the wear scar. These fractions of the phosphorus species were then compared to calibrated polyphosphate compounds with known chain lengths whose peaks have been fitted in the same manner.

X-PEEM was performed using the SPHINX [44] microscope (ELMITEC GmbH) installed on the 6m-TGM (Toroidal Grating Monochromator) beamline at the 1 GeV Aladdin storage ring, University of

Wisconsin, Madison, optimized to give ~0.1 eV resolution at the phosphorus L-edge (for details see refs. [24,44,45]). Image intensity in X-PEEM is proportional to the TEY and the surface sensitivity was limited by the escape depth of the secondary electrons at the phosphorus L-edge (3–5 nm) [45,46]. Spectromicroscopy images were taken with a 0.2 eV step size from high energy to low energy. A 100 μm field of view was chosen for the selected area with a resolution of ~200 nm per pixel. The images were combined to produce a three-dimensional data set or spectromicroscopy “stack” [47] that was analyzed to extract detailed chemical information about the tribofilm using aXis2000 software [47,48]. The software allowed for selection of regions of several pixels in size to extract XANES spectra. Stacks were acquired at the phosphorus L-edge (130–160 eV) and analyzed for differences in chemistry. Unfortunately, the signals acquired at the sulfur (155–190 eV), silicon (120–195 eV), and aluminum (65–90 eV) L-edges generally were too weak to obtain meaningful spectra. Silicon and aluminum are covered with a layer of the tribofilm (thickness > 10 nm) and which thus masks the silicon and aluminum signal.

2.4. Nanomechanical property and wear acquisition

The mechanical properties of the substrate and antiwear films were investigated using a Hysitron Tribo-scope®. This system has the capability to image a surface directly before and after indenting, using the force transducer. Details of the specific instrumentation and setup are given elsewhere [31]. An AFM J-scanner was used to image the surface. The three-sided diamond Berkovich indenter with an elastic modulus (E_i) between 1000–1140 GPa, a Poisson ratio (ν_i) of 0.07 and a tip radius of curvature between 110 and 130 nm was used for all indentations. Topographic images were taken before and after indenting a region. A certain preset force was applied and the resulting depth of penetration of the indenter is recorded. Both the loading of the preset force and unloading was monitored. The elastic modulus was extracted using the Oliver-Pharr method [49] from the unloading section of the force-distance (f - d) curve. The range of applied loads studied was 30–300 μN.

The wear scar width (WSW) of the steel pins was measured using a calibrated optical Zeiss Axioplan microscope over 10 random regions along the length of the pin. The wear scar depth (WSD) on the disk was measured using a Tencor® P-10 Surface Profiler which sampled 10 arbitrary regions along each wear scar and the depths were averaged. These values of WSW and WSD were used as a measure of wear performance.

3. Results and discussion

3.1. Surface analysis of the substrate and tribofilms

AFM was used to examine the local morphology of the tribofilms before and after a rubbing experiment. The polishing procedure with the $0.03\ \mu\text{m}$ alumina paste resulted in a mirror finish. A representative $40 \times 40\ \mu\text{m}^2$ AFM image after mechanical polishing is shown in figure 1(a). The heterogeneous surface has an average roughness (R_a) and root mean squared (RMS) roughness (R_{RMS}) of 29 ± 7 and 34 ± 8 nm, respectively. The regions colored in yellow (high regions) are believed to be silicon grains, and the darker regions are attributed to possible cavities in the surface as a result of the removal of Si grains by the polishing procedure. It is difficult to distinguish the grains of silicon and the aluminum matrix after polishing (figure 1(a)). This is attributed to the polishing procedure, in which the aluminum matrix is more readily defaced than the harder silicon phase.

It is clear that after a 30 s etch in 5% NaOH (figure 1(b)) two distinct phases can be identified. One is the aluminum matrix (red), and the other is the silicon grains (yellow) which was confirmed by EDX. The Si grains are raised ~ 370 nm above the aluminum rich matrix after etching for 30 s and the height increases considerably with etching time (after etching for 15 or 45 s the Si grains are raised ~ 187 and ~ 633 nm above the aluminum matrix, respectively).

The silicon grains are approximately $4\text{--}7\ \mu\text{m}$ in size; however “agglomerations” of silicon grains may appear larger than $7\ \mu\text{m}$ in figure 1(b). The surface coverage of the Si grains was estimated as $44 \pm 2\%$; however this is an overestimation, based on the convolution of tip interaction with the raised Si grains.

Figure 1(c) shows an AFM image of a tribofilm generated on a 30 s etched surface (tribofilm A, table 2). Four reference markings are shown (a, b, c, and d). These represent identifiable features which will be used to compare information from several techniques. It is evident that the surface is quite heterogeneous, although many observations can be made. Large grains are found that resemble Si on the pristine surface. Regions in between Si features appear to be heterogeneous. From figure 1(c), it can also be seen that some pitting has occurred (two examples are shown), and wear debris has become embedded in the film.

In previous studies similar features were observed [36] and were explained as the result of a large normal force and resulting tangential force from sliding which accounted for the elongation of the pads in the sliding direction. However we do not see the formation of large pads ($> 10\ \mu\text{m}$) elongated in the sliding region as was observed from the tribochemical decomposition of ZDDP on steel surfaces [36]. Several regions were imaged over many samples (not shown) and the results

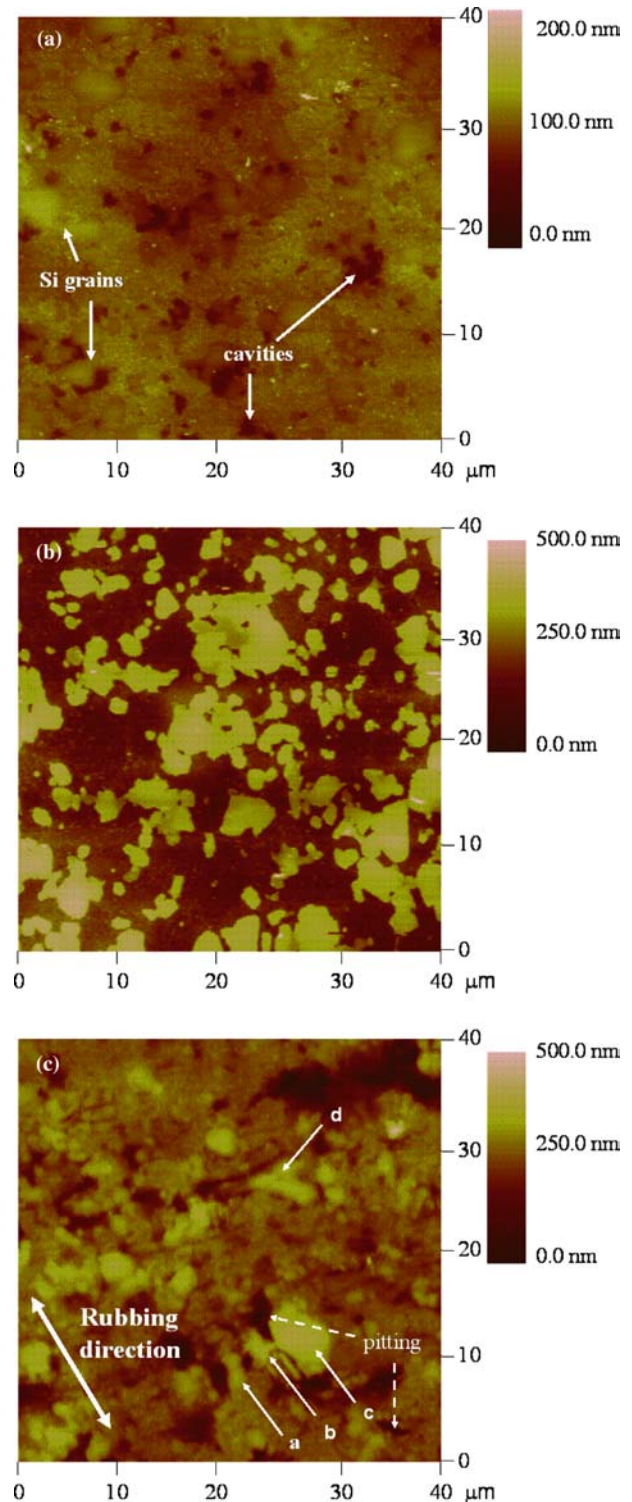


Figure 1. Representative contact AFM images of Silitec 5TM after (a) mechanical polishing, (b) after a 30 s in 5% NaOH, and (c) after tribofilm formation. Regions of interest are shown (a, b, c, & d) and can be compared to the same location in figures 7, 8, and 10. Representative $40 \times 40\ \mu\text{m}^2$ contact AFM image of tribofilm A.

were consistent, indicating that formation of larger pads was rare, although some pads appeared larger than others which were attributed to be agglomerations of

smaller pads, similar to the substrates silicon grain size (figure 1(b)).

These non-uniform films have a height profile lower than previously established from the etching (figure 1(b)). This could be attributed to a number of different causes related to the rubbing. For example the Si grains could be worn down or compressed into the Al matrix, or perhaps film and/or debris was formed and/or transferred from Si on the Al matrix.

3.1.1. Phosphorus K-edge XANES

Figure 2 shows the phosphorus K-edge XANES spectra, collected in the TEY mode, of three tribofilms, compared to unreacted ZDDP and model compounds $Zn_4P_6O_{19}$ and $AlPO_4$. Also included is an example of peak fitting performed on the P K-edge spectra for tribofilm A to determine the relative percentages of each phosphorus species present.

A strong single intense peak is characteristic of the phosphorus K-edge, which is attributed to the transition of a phosphorus 1s electron to an empty p-like anti-bonding state. As shown in figure 2, ZDDP's main peak a, is observed at ~ 2149.4 eV, while the main peak in the tribofilms, resulting from the decomposition of ZDDP into a polyphosphate glass, peak b, is observed at

2152.0 eV. The difference of ~ 2.5 eV is in accordance with previous results on steel surfaces [31].

The structure of ZDDP has the phosphorus atom coordinated to two sulphur and two oxygen atoms, while the phosphorus atom in $Zn_4P_6O_{19}$ is coordinated to four oxygen atoms. The shift in energy between ZDDP and $Zn_4P_6O_{19}$ has been attributed to the difference in electronegativity between sulphur and oxygen [31]. The oxygen induces a peak shift to a higher binding energy.

Tribofilm A was made under a standard set of conditions (table 2), tribofilm B was made at 200 °C, and tribofilm C was made with 0.3% ZDDP, while all the other conditions remained constant. There is a distinct shift in energy from both $Zn_4P_6O_{19}$ and $AlPO_4$ compared to the main peak of tribofilm A of ~ 0.2 and ~ 0.8 eV, respectively. The pre-edge shoulder on the tribofilm, labeled peak a, corresponds to unreacted ZDDP, which was significantly present for all studies that contained 1.2% ZDDP or a higher concentration. At 200 °C (tribofilm B), the pre-edge shoulder is very small, suggesting that ZDDP has degraded at such high operating temperatures and the polyphosphate structure is the predominant phosphorus species observed.

The unreacted ZDDP peak, peak a, was small for all conditions in which 0.3% ZDDP was examined

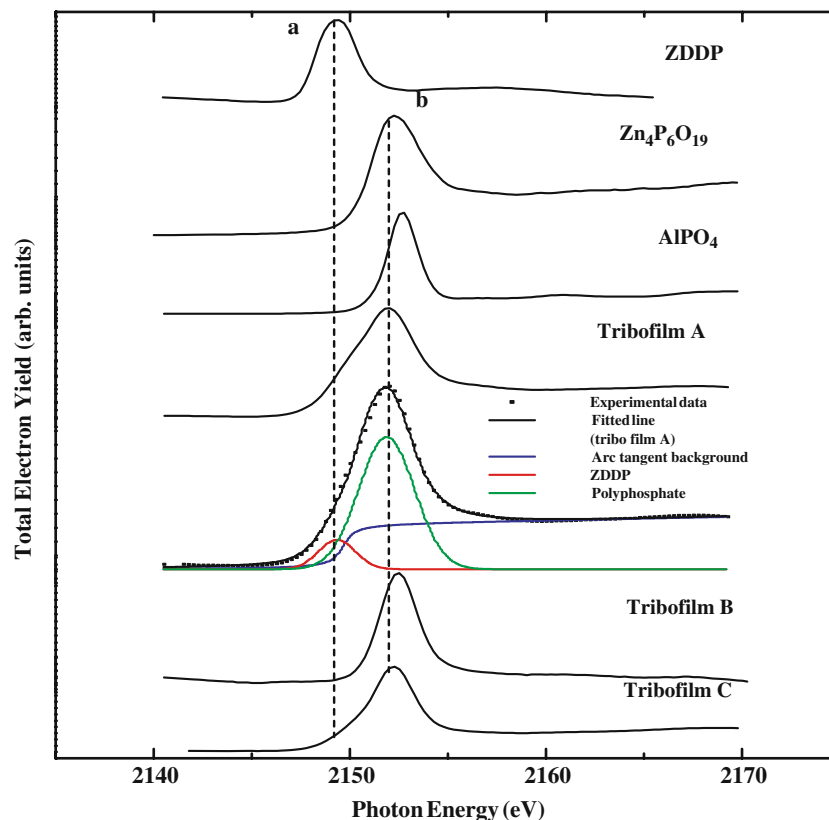


Figure 2. Phosphorus K-edge XANES spectra of unreacted ZDDP, model compounds $Zn_4P_6O_{19}$ and $AlPO_4$ and three tribofilms. Tribofilm A was made under the standard conditions. An example of peak fitting for tribofilm A performed on the P K-edge data to determine each of the phosphorus species detected in the wear scars is included. Tribofilm B was made under the standard conditions except at 200 °C, and tribofilm C was made using a 0.3% ZDDP solution.

Table 2.
Physical parameters for a 30 s etched substrate

Tribofilms	Tribofilm conditions
Tribofilm A	30 min, 100 °C, 100 N, 1.2% ZDDP solution
Tribofilm B	30 min, 200 °C, 100 N, 1.2% ZDDP solution
Tribofilm C	30 min, 100 °C, 100 N, 0.3% ZDDP solution
Tribofilm D	720 min, 100 °C, 100 N, 1.2% ZDDP solution

Note: Tribofilms B–D were made with the same conditions as tribofilm A with the exception of one parameter changed.

(tribofilm C). Peak a, was present for 0.6% ZDDP at the shortest rubbing time (5 min), but undetectable for longer times (spectra not shown).

Table 3 shows the de-convoluted peak areas from the phosphorus K-edge spectra achieved from peak fitting, which estimates the percentage of unreacted ZDDP and polyphosphate glass formed comparing rubbing times, rubbing temperatures and initial ZDDP concentrations, independently. An example of the de-convoluted peak areas can be found in figure 2 for tribofilm A; details of the procedure can be found elsewhere [42,43,50].

It can be seen that with increasing rubbing time and rubbing temperature, the amount of unreacted ZDDP diminishes, suggesting that ZDDP depletes with operating time and higher temperatures. Table 3 shows another interesting trend, as the concentration increases, the percentage of unreacted ZDDP increases when rubbed for a given time.

Other results from the de-convolution of peak areas from the phosphorus K-edge XANES spectra (not shown) indicate that the etching time and applied load do not change the amount of unreacted ZDDP (~8–9%) and the yielded spectra is similar to that of tribofilm A in figure 2.

Nicholls *et al.* [43] studying other Al–Si alloys, A319 (~7% Si), A6061 (~0.7% Si), under low-load

boundary lubrication conditions found a pre-edge peak (~2145.5 eV) and a pre-edge shoulder (~2150.1 eV) in the P K-edge spectra, which was attributed to the formation of a phosphide and a combination of unreacted ZDDP and a linkage isomer (LI), respectively. It was suggested that the formation of the phosphide is mediated by nascent aluminum formed from wear asperities [43]. Neither the phosphide peak, nor the LI shoulder was observed with the Silitec 5TM alloy, for all conditions tested. Similar findings were observed for A390 (16–18% Si) [30] and rationalized in terms of the idea that the larger Si grains reduced the formation of the phosphide below the detection of the spectroscopy, by minimizing the contact of the nascent aluminum with the steel pins. This is a very plausible rationale as the Silitec 5TM alloy has a higher silicon weight content, and the etching procedure prior to the wear tests ensured that the Si grains protrude from the surface by at least 180 nm, effectively minimizing the steel pin contact with the aluminum matrix.

The film thickness can be calculated from the XANES spectra at the phosphorus K-edge according to a method described elsewhere [51]. A linear relationship was found between the height of the phosphate peak on the P K-edge FY spectra and the phosphorus areal density obtained from particle induced X-ray emission (PIXE) elemental analysis technique assuming that zinc pyrophosphate ($Zn_2P_2O_7$) with a density of 3.75 g/cm^{-3} is exclusively formed. Using the described method [51], the average film thickness was found to range between 40 and 225 nm. The thickness was found to generally increase with concentration. Changes in the etching time of the substrate, and the applied load seemed to have little effect on the film thickness ($120 \pm 20 \text{ nm}$). A saturated thickness of around ~225 nm, which evolves after rubbing for more than 30 min, was found.

Table 3.

De-convoluted peak area percentage from peak fitting of the phosphorus K- and L-edge XANES spectra comparing various rubbing times, rubbing temperatures and ZDDP concentrations. All experimental parameters were made under standard conditions of tribofilm A (table 2) except for the one studied.

Rubbing time (min)	Rubbing temperature (°C)	ZDDP concentration (%)	P K-edge XANES		P L-edge XANES	
			Unreacted ZDDP (%) ~2149 eV	Polyphosphate glass formed (%)	Ratio of peaks a/c	Ratio of peaks b/c
5	100	1.2	9.5 ± 0.5	90.5 ± 0.5	0.45	0.40
30	100	1.2	8.8 ± 0.4	91.2 ± 0.4	0.47	0.43
180	100	1.2	7.5 ± 0.2	92.5 ± 0.2	0.51	0.44
720	100	1.2	2.3 ± 1.8	97.7 ± 1.8	0.63	0.54
30	100	1.2	8.8 ± 0.4	91.2 ± 0.4	0.47	0.43
30	150	1.2	3.4 ± 1.4	96.6 ± 1.4	0.46	0.41
30	200	1.2	2.6 ± 0.5	97.4 ± 0.5	0.36	0.32
30	100	0.3	3.3 ± 0.9	96.7 ± 0.9	0.45	0.39
30	100	0.6	6.3 ± 0.8	93.7 ± 0.8	0.47	0.42
30	100	1.2	8.8 ± 0.4	91.2 ± 0.4	0.47	0.43
30	100	2.0	10.0 ± 1.4	90.0 ± 1.4	0.48	0.44

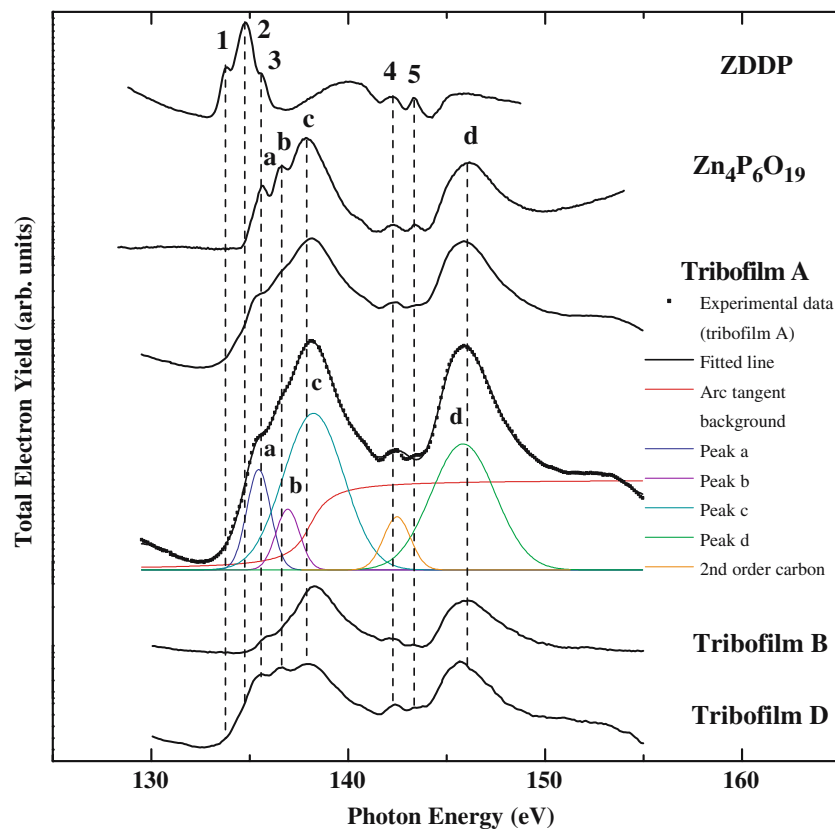


Figure 3. Phosphorus L-edge XANES spectra of unreacted ZDDP, model compound $Zn_4P_6O_{19}$, and three tribofilms. Tribofilm A was made under the standard conditions. An example of peak fitting for tribofilm A performed on the P L-edge data to determine the relative peak heights of peaks a, b, and c is included. Tribofilm B was made at 200 °C, and tribofilm D was rubbed for 720 min.

3.1.2. Phosphorus L-edge XANES

Figure 3 presents the phosphorus L-edge spectra for unreacted ZDDP, model compound $Zn_4P_6O_{19}$, and three tribofilms. Also included is an example of peak fitting to determine the area and amplitude of each peak present in the P L-edge. A detailed description can be found elsewhere [24,42]. The L-edge offers richer information compared to the K-edge spectra. The L-edge is characterized by spin-orbit splitting of the phosphorus 2p electrons and excitation to anti-bonding orbitals. Peaks labeled 1 and 2 (and a & b) are attributed to the transitions from the $2p_{3/2}$ and $2p_{1/2}$ to the a_1^* anti-bonding orbital [52]. The 2p spin-orbit splitting was measured as 0.8 eV, corresponding well with the literature value of 0.86 eV [52]. Peak 3 (and c) is attributed to the transition of the phosphorus 2p electrons to the t_2^* molecular orbital. Peak d, known as a shape resonance peak, located at ~ 146 eV, is only present when phosphorus is coordinated to three or more electronegative atoms, such as oxygen [18]. The shape resonance peak is characteristic of all phosphates regardless of structure, whether crystalline or glassy [18]. The peaks labeled 4 and 5, at ~ 142.2 eV are attributed to a second-order carbon contamination of the sample and the beamline optics. According to the L-edge XANES spectra of the tribofilms made under the different conditions, it can be

confirmed from peaks a–d, that a polyphosphate has formed.

The slight shift in energy from all spectra shown is due to variations in the formal charge of the metal cations on the oxygen surrounding the phosphorus.

The shoulder labeled 2 in the spectra of the tribofilms corresponds to unreacted ZDDP. It is evident that there is unreacted ZDDP present for the standard conditions, and also when a sample is rubbed for 720 min (tribofilm D). At 200 °C (tribofilm B), the shoulder is absent indicating that at higher temperatures most of the ZDDP has been consumed and reacted.

The de-convoluted intensity of peaks a and b relative to peak c achieved from peak fitting, has been found to vary depending on polyphosphate chain length [18]. Yin *et al.* [18] have shown that the ratio of peaks a/c and b/c increase with increasing polyphosphate chain length (see table 3). Although the various spectra look different, it was found that most of the tribofilms are comprised of mainly medium to short chain polyphosphates. Nicholls *et al.* [24] have provided a calibration curve assigning the a/c and b/c ratios to the number of phosphorous atoms in different chain-length polyphosphate glasses. We have assigned short chain polyphosphates to have 10 or fewer P atoms in a polyphosphate glass corresponding to an a/c ratio of ~ 0.44 or less. Long chain polyphosphate

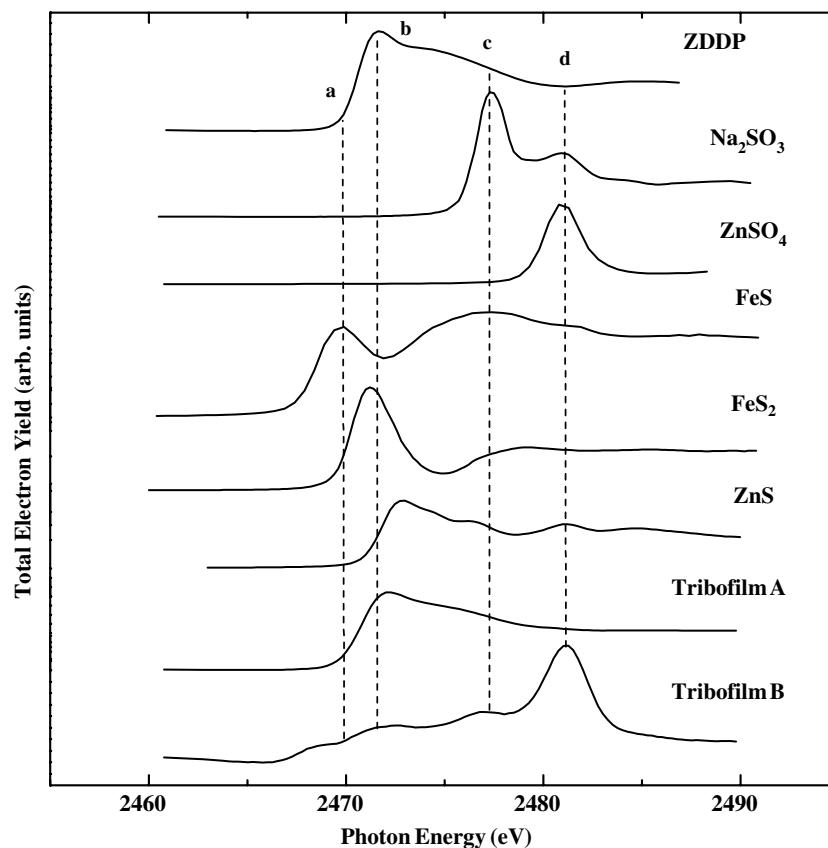


Figure 4. Sulphur K-edge XANES spectra of unreacted ZDDP, model compounds Na_2SO_3 , ZnSO_4 , FeS , FeS_2 , ZnS , and two tribofilms. Tribofilm A was made under the standard conditions and tribofilm B was made at 200°C .

species are characterized by 25 or more P atoms in the polyphosphate chain length, resulting in an a/c ratio of ~ 0.60 or greater. Medium to short chained polyphosphates therefore have an a/c ratio between ~ 0.44 and ~ 0.60 , and have between 10 and 25 P atoms in each chain in the polyphosphate glass network.

Higher temperatures (tribofilm B) were found to be overwhelmingly comprised of shorter chained polyphosphates (< 10 polyphosphate units), consistent with observations made by Yin *et al.* [18] for 30 min. antiwear films rubbed onto steel at high temperatures. The spectrum of tribofilm A has been fitted to an intermediate mixture of short to medium-chained polyphosphates (10–25 polyphosphate units). The spectrum of tribofilm D was best fitted with longer chain polyphosphates (> 25 polyphosphate units), also consistent with results from Yin *et al.* [18] for antiwear films prepared on steel substrates for longer rubbing times. All other tested conditions gave spectra similar to that of tribofilm A in figure 3.

It is apparent from the P L-edge XANES spectroscopy that higher temperatures yield shorter chain polyphosphates, while milder conditions generate a mixture of medium and shorter chain polyphosphates, and longer rubbing times generate longer chain polyphosphates.

3.1.3. Sulphur K-edge XANES

Figure 4 shows the sulphur K-edge XANES spectra collected in TEY mode comparing unreacted ZDDP, Na_2SO_3 , ZnSO_4 , FeS , FeS_2 , ZnS and two tribofilms. The peak positions are shown in table 4. The shift of the white line is attributed to the local environment of the sulphur atom, and its oxidation state. Comparing the spectra of ZDDP (peak b) and Na_2SO_3 (peak c), there is a shift to higher energies, resulting from an increase in the oxidation number of the absorbing atom.

Comparing spectra of tribofilms A and B with the model compounds, it appears that at higher temperatures, the sulphur content of ZDDP transforms to form

Table 4.
Peak positions of S K-edge XANES spectra of model compounds and tribofilms (± 0.1 eV).

Samples	S K-edge (eV)
ZDDP	2471.8
Na_2SO_3	2477.3
ZnSO_4	2480.8
FeS	2469.9
FeS_2	2471.3
ZnS	2472.9
Tribofilm A	2472.5
Tribofilm B	2481.28

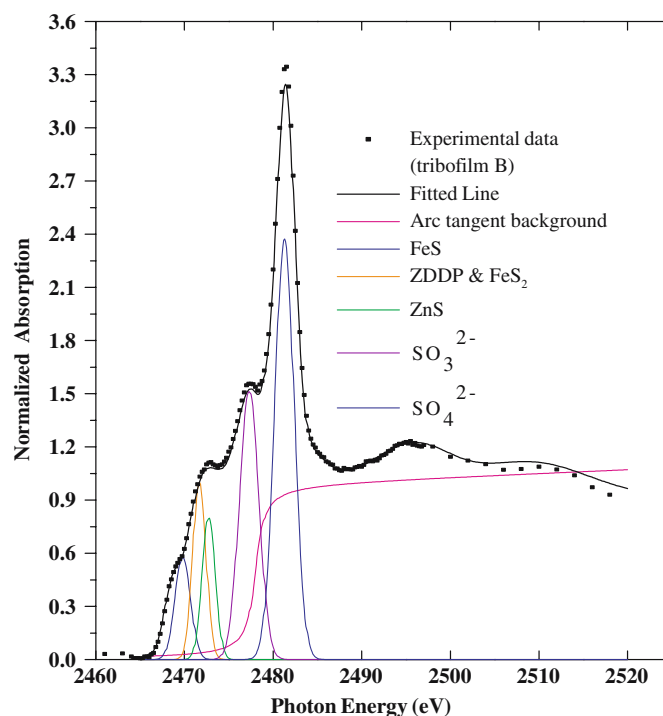


Figure 5. An example of the peak fitting performed on the sulfur K-edge XANES spectra to determine the relative percentages of each sulphur species detected in the wear scars. This example is for a sample rubbed at 200 °C (tribofilm B).

sulphate and small amounts of other species. Under less extreme operating conditions, the sulphur content is present as the reduced species (ZnS) as observed previously [18,53–55].

A semi-quantitative measurement of the types of sulphur present in the antiwear films can be made based upon the cross section of the sulphur species. Details of the procedure are given by Huffman *et al.* [50]. Figure 5 is an example of the fitting results for tribofilm B. The sulphur species were fitted with peaks for FeS, ZDDP & FeS₂, ZnS, SO₃²⁻, and SO₄²⁻. Only one peak was fitted for unreacted ZDDP and FeS₂, and added to the peak for ZnS because as seen in the spectra (figure 5), the peaks are not well resolved and the energy difference between the three compounds (table 4) is very close to the photon resolution of the beamline.

Table 5 shows a summary of the approximate percentages found for each of the sulphur species present. The presence of FeS (~8.2%) indicates iron transfer from the steel pin to the disk under extreme operating conditions. It is appears that under these conditions, the

ZDDP additive was not protecting the surface properly and the wear rate is high as wear debris from the disk is detected in the film in the form of FeS, since there is no iron content in the alloy.

All the tribofilms made under all the tested conditions gave spectra similar to the one obtained for tribofilm A, with the exception of the sample rubbed at 200 °C (tribofilm B). Our results show that signal for sulphur was typically much weaker, compared to the phosphorus signal, indicating that the film is deficient in sulphur content which is in accordance with previous studies [18,56].

3.2. Wear scar widths and profilometry

From the rubbing experiments, a wear scar depth (WSD) is generated on the disk and a wear scar width (WSW) is left on the steel pin that can be correlated to give a qualitative measurement of the wear.

Figure 6 shows the WSD and WSW plotted as a function of rubbing time (standard conditions were used

Table 5.

De-convoluted peak area percentage of the sulphur K-edge spectra. All spectra were similar to tribofilm A for all conditions tested except for the tribofilm made at 200°C (tribofilm B) (see figure 8).

Samples	FeS (%) 2469.9 eV	Unreacted ZDDP (2471.8 eV), ZnS (2472.9 eV) & FeS ₂ (2471.3 eV) (%)	SO ₃ ²⁻ (%) 2477.3 eV	SO ₄ ²⁻ (%) 2480.8 eV
Tribofilm A	0	~100	0	0
Tribofilm B	~8.2	~21.9	~27	~42.9

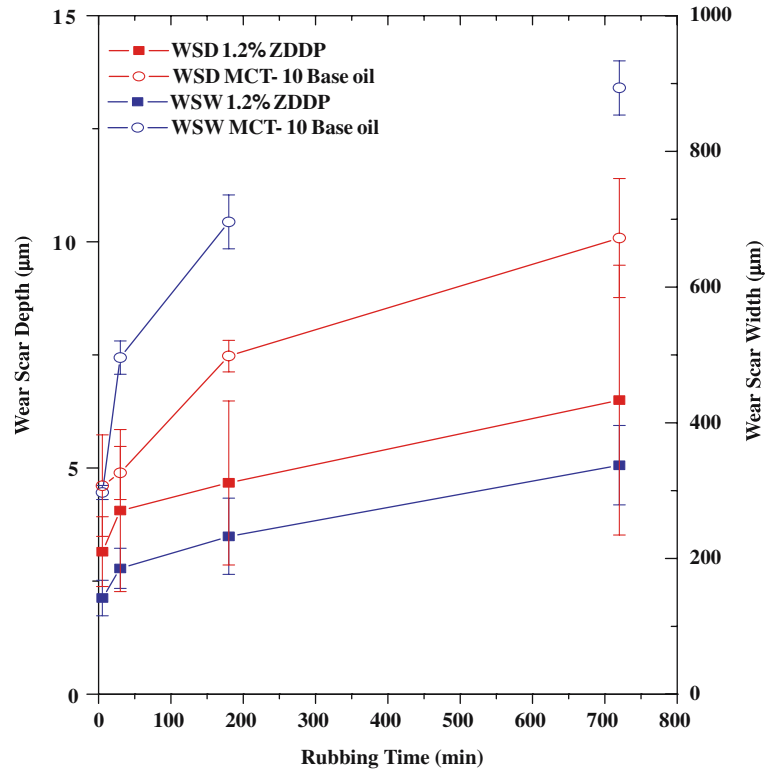


Figure 6. Comparison of wear using base oil, with or without ZDDP. The wear scar depth (WSD) measured on the disk and wear scar width (WSW) measured on the 52100 steel pin are presented as a function of rubbing time. All presented values were obtained under the standard conditions, with exception of varying rubbing time.

except for rubbing time). It can be seen that the WSD even after short rubbing times are larger than the Si grain heights after the etching process (~ 370 nm). This may suggest a compression of the Si grains into the matrix, or a significant amount of wear of the Al–Si disk, or most likely, a combination of both.

Another prominent characteristic is that when ZDDP is used the WSD was decreased by $1 \mu\text{m}$ for all studied rubbing times. The results also show that the WSW increases with time, compared to base oil alone (by at least a minimum of $160 \mu\text{m}$).

Nicholls *et al.* [31] using the same type of pin and experimental set-up found a WSW of $\sim 112 \mu\text{m}$ on steel (60 min, 220 N, all other conditions were similar to tribofilm A) using 1.2% ZDDP and $\sim 227 \mu\text{m}$ WSW using base oil alone. Our results have shown that after 5 min, the WSW is $141.6 \pm 26.2 \mu\text{m}$ using a 1.2% ZDDP solution, and $297.4 \pm 10.3 \mu\text{m}$ in base oil alone. Comparing the experiments, it is evident that after 5 min, more wear has occurred on the 52100 steel pin using the Silitec 5TM alloy disk compared to a 60 min experiment with a steel/steel pin and disk couple using a higher force. This result can be attributed to the specific topography of the Silitec 5TM disk in which the etched Si grains must support the whole applied load. It could be possible that after the etching, some Si grains are loosely embedded in the matrix causing some Si grains are plucked out of the

matrix and acting as third body abrasives leading to an increase in the WSW of the steel pins.

Results from the other studied parameters (variation of load, etching time, temperature, concentration) show that using a ZDDP solution consistently reduces wear compared to rubbing in base oil alone.

3.3. Physical interpretation of wear mechanisms

From just the XANES spectroscopy, it is difficult to evaluate the ideal conditions for the optimum antiwear protection. A good measure of prolonged surface protection is the percentage of unreacted ZDDP to ensure tribofilm renewal and the least amount of iron detected in the film, originating from the steel pin.

Nicholls *et al.* [43] outlined four requirements for sustainable polyphosphate film formation for steel/steel contact. The first is that the temperature of the contact zone must be high enough to transform ZDDP to form an antiwear film. The three studied temperatures (60, 100, 200 °C) produced a polyphosphate film, satisfying the first condition. The second requirement deals with the similarity of the mechanical hardness and strength of the metal/metal couple. Although the Young's modulus for steel and Silitec 5TM are different, the aluminum matrix is etched away and the Si grains are left exposed to provide a rigid

surface that withstands high pressures and shear forces. The steel pin rubbing against the Si grain is then supported, satisfying the second condition for polyphosphate film formation. The third condition states that the strength of the film formed between the metal/metal couple must be less than that of the surfaces in contact (discussed in a later section). The fourth condition states that there must be no abrasive third body in the contact zone. The presence of iron is related to material transfer, which signifies poor antiwear properties of the film and a possible introduction of an abrasive third body. Nicholls *et al.* [43] have documented that other Al–Si alloys (A319 & A6061), the Si particles act as asymmetric abrasives that can become dislodged which is also responsible for scuffing, thus not satisfying condition four. The same observations in these experiments accounts for the increase in the WSW as previously mentioned (condition four is not satisfied).

We propose a fifth condition for sustainable film formation relating the adhesion of antiwear films to the substrate. It has been suggested that phosphates bind to the surface via oxide on steel surfaces [21,43]. Zhang *et al.* [54] have found that phosphate formation is due to the oxide layer on the surface. The authors have shown that the oxide layer on the steel surface facilitates the decomposition of ZDDP to phosphate. Iron oxide is known to be quite thick on steel surfaces and as a result, promotes and prolongs the film stability and formation. However, silicon and aluminum oxides are very thin ($\sim 1\text{--}3$ nm) and may not play a significant role in the adhesion of the antiwear film to the silicon grains embedded in the aluminum matrix. Due to the heterogeneous nature of the substrate after the etching procedure which results in a varying topography, it is very difficult to ascertain adhesion properties. However, this model is used to explain why the wear scar width of the pin and wear scar depth on the disk (figure 6) increase as the rubbing times increases. The antiwear film does not adhere to the substrate as well as it does adhere to steel, therefore not satisfying condition five.

Comparing the XANES spectroscopy and considering these five proposed conditions for adequate antiwear performance, the ideal conditions for tribofilm formation is a milder operating environment. Lower temperatures (< 200 °C), and shorter rubbing time (< 720 min) results in more unreacted ZDDP (table 3) which could be used to sustain tribofilm renewal and less wear (figure 6—pertaining to the rubbing time discussion) is a good measure of antiwear performance.

3.4. Phosphorus X-PEEM and SEM/EDX mapping

Figure 7(a) is a secondary electron X-PEEM image of tribofilm A obtained at 130 eV. The topography and variable thickness of the different regions of the film demonstrate differential charging and thus the X-PEEM

image does not exactly resemble the AFM image (figure 1(c)). The tribofilms, composed of polyphosphate glasses, are non-conducting, and thus are subject to charging and suppression of secondary electron emission [57]. Furthermore, shadowing also creates artifacts, which also contributes to certain regions of the image appearing darker [37]. Figure 7(b) is a phosphorus X-PEEM distribution map obtained, using the internal model spectra shown in figure 7(c). The internal model spectra are contrasted spectra obtained from individual pixels or regions on the image, and pixels are matched to spectra throughout the image.

Details of the X-PEEM analysis of antiwear films can be found elsewhere [24,37]. The spectra were obtained by analyzing the image sequence from the phosphorus L-edge stack by choosing pixels on the image. Figure 7(c) compares the internal model spectra with the spectra of model compounds ZDDP and $\text{Zn}_4\text{P}_6\text{O}_{19}$. By use of a signal mask that was generated for each component, corresponding spectra for each component were extracted from multiple pixels and averaged [37]. Component maps were generated, and regions corresponding to the long- (yellow) and short- (blue) chain polyphosphate distributions were constructed (figure 7(b)). Bright blue areas correspond to regions where the spectra resemble a short chain polyphosphate, and bright yellow indicates the locations of long chain polyphosphates. Mixtures of short and long chain polyphosphates appear as a dull yellow or grey. Black areas indicate the absence of a good fit, either to long or short chain polyphosphate spectra. It can be seen that the distribution image is primarily composed of short chain polyphosphates, with localized regions of long chain polyphosphates.

The pre-edge shoulder on the extracted spectra for the long and short chain polyphosphate (figure 7(c)) labeled s, is due to unreacted ZDDP. The shoulder, s, aligns with the main peak (peak 2) of ZDDP. The shoulder is more appreciable for the short chain species, suggesting that unreacted ZDDP is mainly concentrated in regions where the short chain polyphosphates are forming. Our results agree with the suggestion [30] that unreacted ZDDP may be trapped in the valleys between the antiwear pads, or embedded into the surface of the antiwear pads. It might be inferred that the resiliency [22,24] of these films might originate from the unreacted ZDDP which can replenish the polyphosphate film as it wears away at contact points.

Mapping SEM/EDX of the region studied by X-PEEM was performed to identify the surface and sub-surface components. Figure 8(a) is a field emission SEM image of the same region taken at 5.0 kV to enhance surface sensitivity. Figures 8(b), (c), (d) and (e) are EDX elemental mapping components for phosphorus, silicon, aluminum, and zinc respectively. The brighter areas correspond to an abundance of that element.

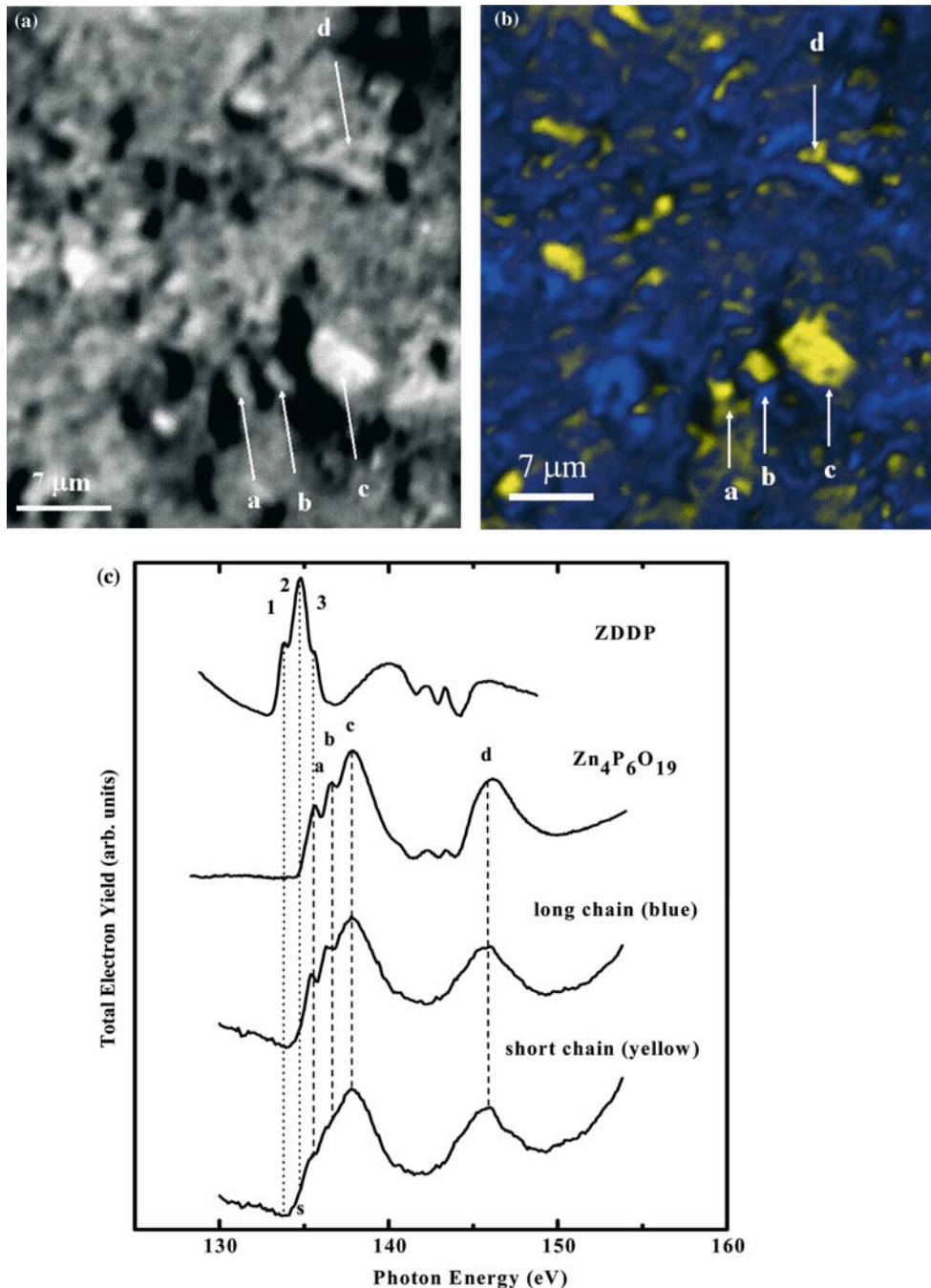


Figure 7. Phosphorus X-PEEM (a) the secondary electron image obtained by the X-PEEM. This image was acquired at 130 eV (b) distribution map of tribofilm A and (c) corresponding spectra. The yellow regions indicate long chain polyphosphates and the blue areas represent regions of short chain polyphosphates. Black areas are regions where the spectra were not fitted well with neither long nor short chain polyphosphate spectra. Regions of interest are shown and can be compared to the same features outlined in figures 1(c), 8 and 10.

The sampling depths of EDX and X-PEEM are substantially different. The X-PEEM sampling depth is $\sim 2\text{--}5$ nm, whereas that of EDX is on the order of at least a 1000 nm (micron) [58]. As a result, bulk silicon is also being sampled, thus certain mapped regions of Si may appear larger on the EDX map compared to the X-PEEM image. However, an interesting correlation

can be made between figures 7(b) and 8(a)–(c); it can be seen that the long chain polyphosphates seem to be preferentially forming on the silicon grains.

AFM topography of the region inspected by X-PEEM for tribofilm A (figure 1(c)), show that the Si grains are raised, suggesting that long chain polyphosphates have formed at stress points, probably due to

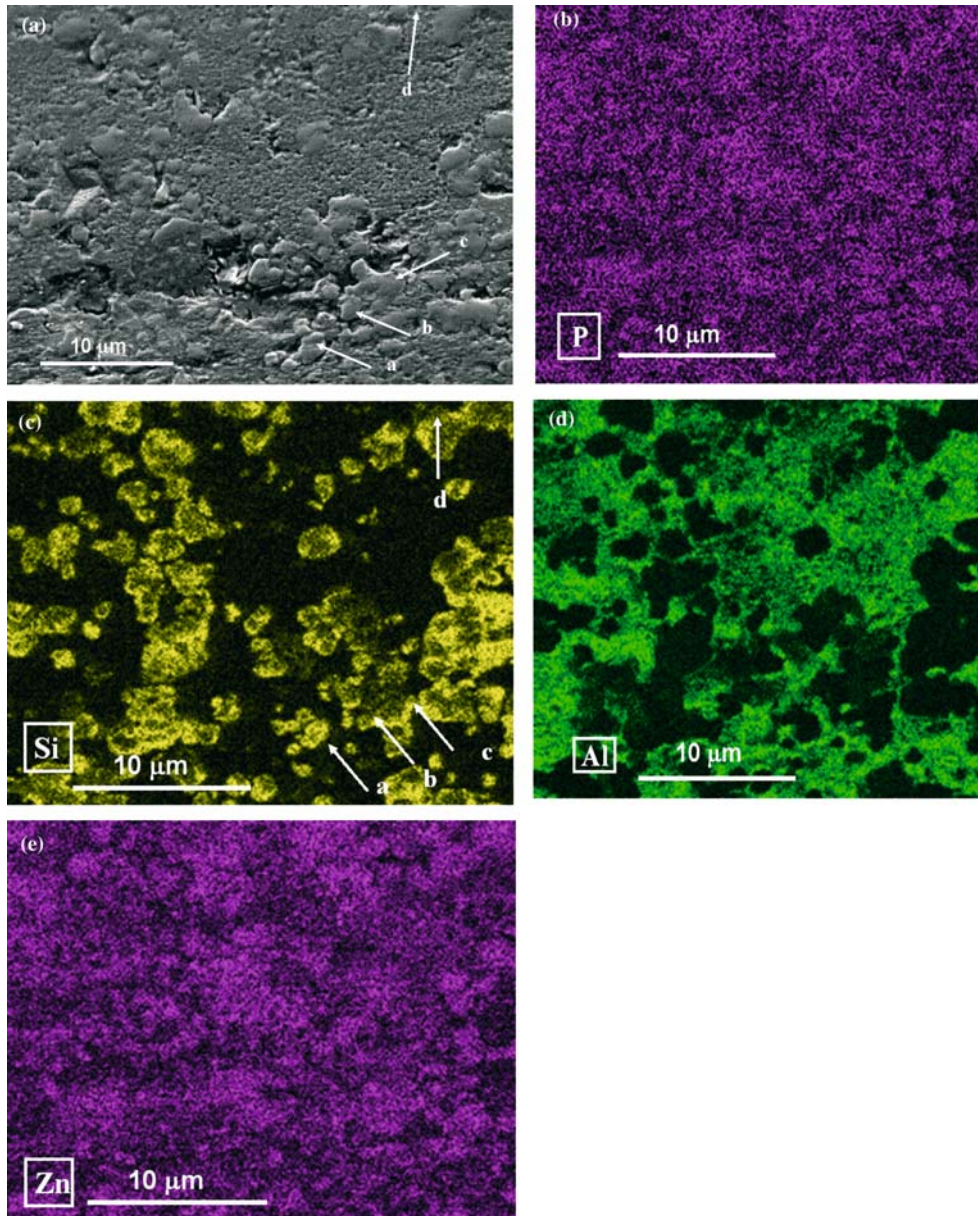


Figure 8. (a) Field emission SEM image and (b)–(e) mapping EDX of a tribofilm where X-PEEM analysis was carried out, at 5.0 kV, and 17 mm working distance. Brighter areas in the EDX map indicate an abundance of the particular element shown.

factors such as elevated contact temperature and friction. The shorter chain polyphosphates and unreacted ZDDP seem to be situated in the lower topographical regions, the latter acting as a reservoir of ZDDP as the Si grains wear away and pristine surface is exposed. Similar findings were observed on steel surfaces, as the bulk of the film was composed of shorter-chain polyphosphates and the near surface region was composed of longer chain polyphosphates [18].

Also comparing figure 8(b) with 8(e), it can be seen that the presence of zinc is highly correlated to locations where the presence of phosphorus is located. However, due to the abundance and dispersion of zinc and phosphorus shown in the maps, it is difficult to discern if this

correlation is associated to the elements of the substrate (Al & Si).

X-PEEM performed on A390 [30] showed that a polyphosphate film of similar nature forms on the Si grains and Al matrix. The etching procedure enhancing the microstructure of the surface is believed to be the reason why the spectra varies from Nicholls *et al.* [30]. The authors [30] suggest that the polyphosphate film found in the matrix region was transferred from the silicon grains during rubbing. In addition no antiwear pads were formed on the Al matrix. Our results agree with the fact that a polyphosphate has formed on the Al matrix probably due to thermal degradation and material transfer.

3.5. Nanomechanical evaluation

Nanoindentation measurements were made on the polished etched substrate and on the tribofilms. Topography images were taken prior to each indent with the same tip. Force–distance (f–d) curves were taken for the substrate at loads varying between 60 and 300 μN . Measurements on the films were made using a load of 30 μN , this reduced the influence of the underlying substrate by maintaining the maximum indentation depth of $\sim 10\%$ [59,60] of the film thickness.

Imaging prior to indenting permitted the selection of a chosen Si grain, the Al matrix, or a region of interest on the tribofilm. Representative f–d curves for 60 μN indents of the Al matrix and a Si grain are shown in figure 9. The f–d curves show the much stiffer elastic response of the Si grains compared to the Al matrix. The large hysteresis seen in the f–d curves of the Al matrix suggests that the Al matrix plastically deforms more readily, and that the Si grain behaves more elastically, at the load applied. The initial jump in the loading portion of the Al matrix curve (at ~ 3 nm depth) is an indication of fracture of the aluminum oxide (shown with an arrow in figure 9).

The reduced modulus (E^*) was calculated from the unloading portion of the f–d curve by a method suggested by Oliver and Pharr [49] which utilizes the initial slope of the unloading curve. The E^* can be related to the Young's modulus of the sample (E_s) through the equation,

$$1/E^* = (1 - \nu_s^2)/E_s + (1 - \nu_i^2)/E_i$$

where E_i is the Young's modulus of the tip and ν_i and ν_s are the Poisson ratios of the tip and sample, respectively.

The values listed in this report for the tribofilms are the indentation modulus (E_s^*) of the sample, given by

$$E_s^* = E_s/(1 - \nu_s^2) = [1/E^* - (1 - \nu_i^2)/E_i]^{-1}$$

in which the tip properties have been removed from the reduced modulus.

The E_s values averaged over many f–d curves for the aluminum matrix and silicon grains are 79 ± 14 GPa and 148 ± 10 GPa, respectively, which are in good accordance with the Young's moduli reported in the literature [61,62] (Al ≈ 74 –80 GPa, Si ≈ 100 –150).

Indentations were performed on the tribofilm in the same region which was studied by X-PEEM. The indents were carried out on regions where long chain polyphosphates were forming (figure 7(b)). Furthermore, it was easier to identify the long chain polyphosphate regions as they had raised defined structures that resembled Si grains. Difficulty arose in indenting the short chain polyphosphate regions as the heterogeneous topography after rubbing influenced the contact area (of the indenter), and typically gave a high scattering in the measured indentation modulus.

Figure 10(a) and (b) show Hysitron height and deflection images of the tribofilm area examined with X-PEEM. The deflection is the derivative of the height,

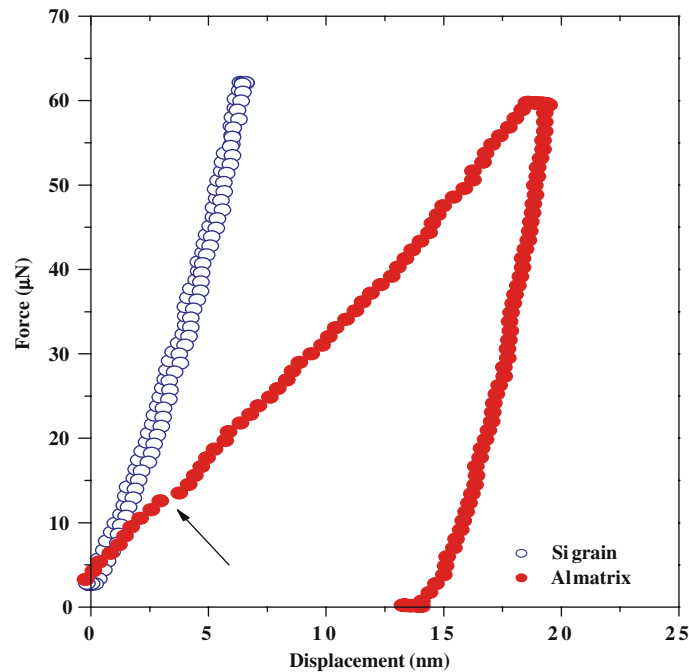


Figure 9. Force–distance (f–d) curves are shown for the polished etched substrate. F–d curves with a maximum load of 60 μN are shown. The ability to image an area prior to measuring an indent with the same tip used for indenting permits selection of either the Al matrix or Si grain. Fracturing of the aluminum oxide layer can be observed in the applied-load portion of the f–d curve (arrow).

and can be used as a better guide to identify flat regions when indenting. Figure 10(c) shows a representative f-d curve obtained on a long chain polyphosphate region formed on a silicon grain.

Qualitatively, the hysteresis of the f-d curve for the tribofilm (figure 10c) shows a mechanical response different from either the Si grains or the aluminum matrix (figure 9). The E_s^* value calculated for long chain polyphosphates was 77 ± 11 GPa which is almost identical to the value given by Nicholls *et al.* [30] for an antiwear pad formed on a Si grain on A390 (76.0 ± 7.1 GPa) and similar to the value given by Warren *et al.* [33] for ridges of small pads formed on steel surfaces (~ 81 GPa). The third condition for phosphate formation (section 3.3) is satisfied as the indentation modulus for the phosphate is less than that of the surfaces in contact.

It is widely believed [24,33,36] that the mechanical properties of these antiwear pads are beneficial for preventing wear of asperities by maintaining a softer sacrificial layer between the rubbing surfaces. This study gives further evidence for such a claim as the modulus reported for the long chain polyphosphates formed on the silicon grains acting as antiwear pads are much softer than the underlying substrate.

4. Summary and conclusions

The chemistry and mechanical response of ZDDPs breakdown products as it forms antiwear films has been investigated and has provided new insight in tribology regarding the lubrication of Al-Si alloys.

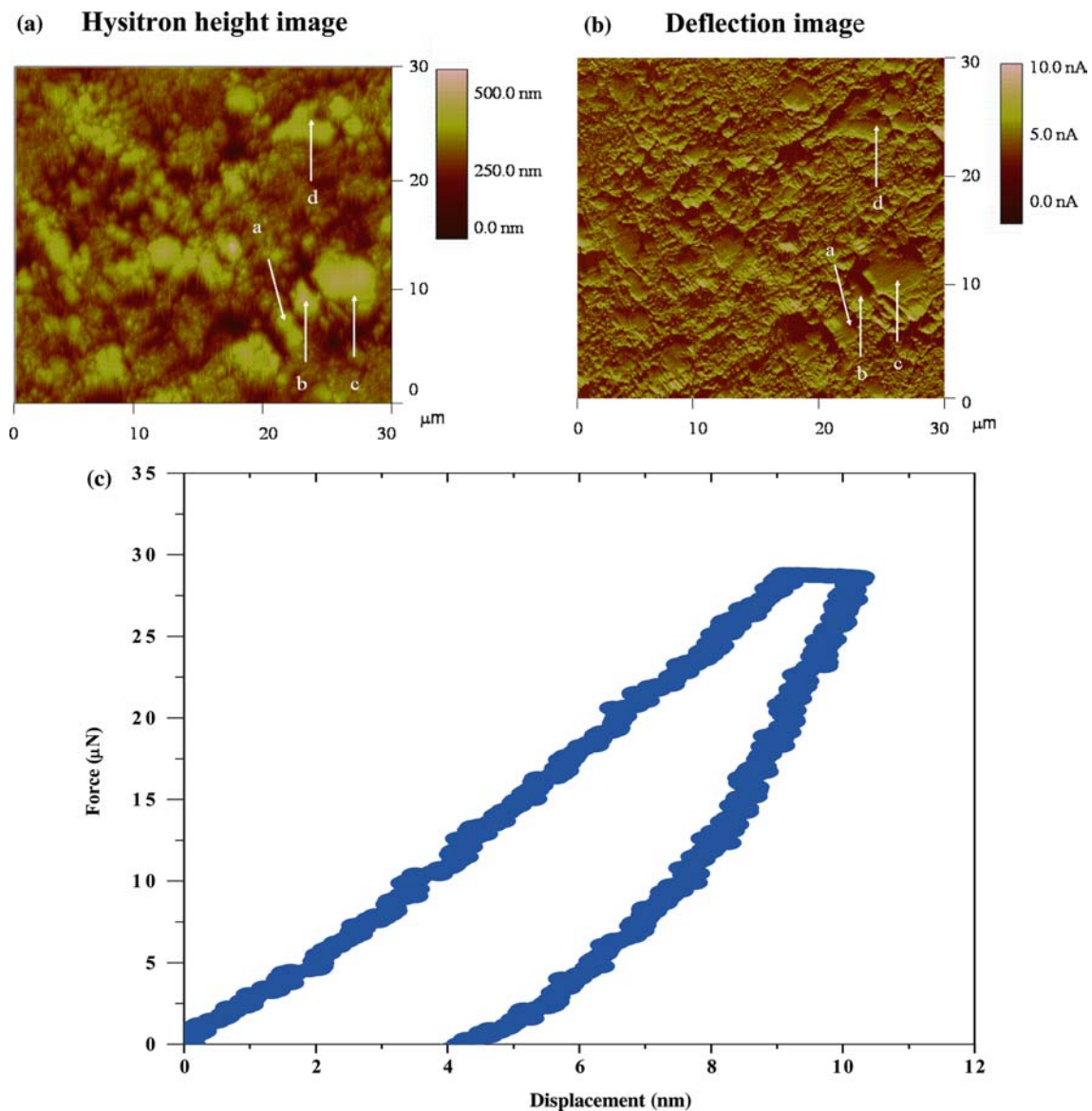


Figure 10. (a) Hysitron height and (b) deflection image of tribofilm region examined by X-PEEM and (c) a representative $30 \mu\text{N}$ f-d curve obtained on a long-chain polyphosphate formed on a Si grain.

We have provided a chemomechanical map of the lubrication of a non-ferrous near hypereutectic Al–Si alloy using ZDDP. This has been performed using AFM topography imaging, SEM/mapping EDX morphology mapping, XANES, X-PEEM, and imaging nanoindentation techniques. Using a grid of fiducial markings to locate the same area, it was found that:

- High resolution AFM imaging provided detailed topographical results concerning the morphology of the bare substrate and the heterogeneous nature of the tribofilm formed as result of rubbing with ZDDP in oil. A correlation was made between etching time and Si grain heights above the aluminum matrix. The tribofilm images showed patchy areas in localized regions, and raised areas which are supposedly load bearing Si grains.
- The analyses from the K- and L-edge XANES spectra reveal that the tribofilms formed on this particular Al-Si alloy were chemically similar, under most conditions, and comprised of polyphosphates of comparable chain length. These tribofilms were similar to those formed on steel. Extreme conditions such as longer rubbing times generated long chain polyphosphates and higher temperatures tended to form shorter chain polyphosphates species determined from spectra peak fitting. The sulphur was mainly found in its reduced form, except at high temperatures where sulphate was the major component generated among other minor sulphur species. No spectral changes were observed with varying applied load and etching time. When the rubbing time increases, the amount of unreacted ZDDP decreased suggesting that ZDDP was consumed with time.
- Polyphosphate film thickness was found to range between 40 and 225 nm.
- X-PEEM coupled with mapping EDX has revealed that long chain polyphosphates were forming exclusively on the raised Si grains, and a mixture of short chain polyphosphates and unreacted ZDDP was found on the Al matrix.
- An indentation modulus of 77 ± 11 GPa was established on the areas where long chain polyphosphates were found, almost identical to the indentation modulus found on antiwear pads formed on Si grains on the A390 alloy. It is generally believed that the tribofilms mechanical response is responsible for the antiwear action, which differs significantly depending on sub-component of the substrate on which it is formed.
- The WSW and WSD findings showed that ZDDP significantly reduced wear compared to the lubrication with base oil alone.

Future work involving lower loads, the effect of different additives and the role of the metal cations could help to better elucidate the role of ZDDP in engine

lubrication. Furthermore, using alternative indentation techniques, such as the interfacial force microscopy (IFM), higher resolution topography imaging and higher load and depth sensitivity at lower loads would be beneficial asset to study and assess the tribofilms mechanical response. Elevated temperature studies could be conducted using an environmentally controlled-IFM (EC-IFM), that could help to explore conditions that are more relevant to automobile engine operating conditions.

Acknowledgments

The authors would like to thank Mr. Ross Davidson and the rest of the staff at Surface Science Western (SSW) for assistance in acquiring the SEM/EDX data. We are also grateful to Mr. Phil Shaw, of the Physics Machine Shop, and to Dr. Leighton Coatsworth both from The University of Western Ontario. We are also obliged to Dr. Kim Tan and Dr. Astrid Jürgensen, from the Canadian Synchrotron Radiation Facility (CSRF), University of Wisconsin, Madison, for their technical support; Imperial Oil of Canada (ESSO) for oil additives; and the National Science Foundation (NSF) for supporting the SRC under grant # DMR-0084402. This work was financially supported by the National Research Council of Canada (NRC) and the Natural Sciences and Engineering Research Council of Canada (NSERC), Centre for Automotive Materials and Manufacturing (CAMM), an agency supported through the Ontario Research and Development Challenge Fund (ORDCF), General Motor of Canada Ltd., General Motors R&D center and Hysitron Inc.

References

- [1] P. Stocker, R. Franz and K. Hummert, *MTZ Motortechnische Zeitschrift* 58(9) (1997) 1.
- [2] D.M. Jacobson and A.J. Ogilvy, *Mat.-wiss. u. Werkstofftech.* 34 (2003) 381.
- [3] K. Hummert, W. Frech and M. Schwagereit, *Metall* 9 (1999) 496.
- [4] J.L. Jorstad, *Trans. Metall. Soc. AIME* 242 (1968) 1217.
- [5] J.L. Jorstad, *Trans. Am. Foundrymen's Soc.* 79 (1971) 85.
- [6] J. Sarabanda, E. Ad. Carvalho and K. Hummert, *The application of rapidly solidified alloys to automotive pistons*, S. Brasil (Mobility Technology Conference & Exhibit, 1993)(Sao Paulo, SAE International, Brasil, 1993) 1.
- [7] A.T. Alpas and J. Zhang, *Wear* 155 (1992) 83.
- [8] X.Y. Li and K.N. Tandon, *Wear* 245 (2000) 148.
- [9] Z. Ma, J. Bi, Y. Lu, H. Shen and Y. Gao, *Wear* 148 (1991) 287.
- [10] M.H. McCay, N. Kennedy, J.A. Hopkins and N.B. Dahotre, *Lasers Eng.* 10 (2000) 107.
- [11] M. Roy, B. Venkataraman and V.V. Bhanuprasad, *Metall. Trans. A* 23 (1992) 2833.
- [12] P.B.N. Bai and S.K. Biswas, *ASLE Trans.* 29 (1986) 116.
- [13] F. Wang, Y. Ma, Z. Zhang, C. Xiaohao and Y. Jin, *Wear* 2004 256 (1992) 342.
- [14] W.J. Bartz, *Engine Oils and Automotive Lubrication* (Marcel Dekker Inc., New York, 1993).
- [15] D. Klamann ed., *Lubricants and related Products: Synthesis, Properties, Applications, International Standards* (Verlag Chemie, Deerfield Beach, FL, 1984).

- [16] K.J. Bird and G.D. Galvin, *Wear* 37 (1976) 143.
- [17] P.A. Willermet, R.O. Carter III and E.N. Boulous, *Tribol. Int.* 25 (1992) 371.
- [18] Z. Yin, M. Kasrai, M. Fuller, G.M. Bancroft, K. Fyfe and K.H. Tan, *Wear* 202 (1997) 172.
- [19] M.L.S. Fuller, M. Kasrai, G.M. Bancroft, K. Fyfe and K.H. Tan, *Tribol. Int.* 31 (1998) 627.
- [20] M. Suominen-Fuller, M. Kasrai and G.M. Bancroft, *Chemical applications of synchrotron radiation*, Advanced Series in Physical Chemistry: Part 2, 2002) Vol. 12B (World Scientific Publishing Co., New Jersey, 2002).
- [21] G.M. Bancroft, M. Kasrai, M. Fuller, Z. Yin, K. Fyfe and K.H. Tan, *Tribol. Lett.* 3 (1997) 47.
- [22] H. Spikes, *Tribol. Lett.* 17 (2004) 469.
- [23] Z. Yin, M. Kasrai, G.M. Bancroft, K.F. Laycock and K.H. Tan, *Tribol. Int.* 26 (1993) 383.
- [24] M.A. Nicholls, P.R. Norton, G.M. Bancroft, M. Kasrai, T. Do, B.H. Frazer and G. DeStasio, *Tribol. Lett.* 17 (2003) 205.
- [25] G. Margaritondo, *Introduction to Synchrotron Radiation* (Oxford University Press Inc., New York, 1988).
- [26] G. De Stasio, M. Capozzi, G.F. Lorusso, P.A. Baudat, T.C. Droubay, P. Perfetti, G. Margaritondo and B.P. Tonner, *Rev. Sci. Instrum.* 69 (1998) 2062.
- [27] H. Ade and S.G. Urquhart, *Chemical applications of synchrotron radiation*, Advanced Series in Physical Chemistry, 2002) Vol. 12A–12B(World Scientific, River Edge, NJ, 2002)edn. 1.
- [28] G. De Stasio, B. Gilbert, O. Fauchoux, M. Capozzi, P. Perfetti, G. Margaritondo and B.P. Tonner, *Rev. Sci. Instrum.* 70 (1999) 1740.
- [29] G.W. Canning, M.L. Fuller, G.M. Bancroft, M. Kasrai, J.N. Cutler, G. De Stasio and B. Gilbert, *Tribol. Lett.* 6 (1999) 159.
- [30] M.A. Nicholls, G.M. Bancroft, P.R. Norton, M. Kasrai, G. De Stasio and L.M. Wiese, *Tribol. Lett.*, submitted for publication.
- [31] M.A. Nicholls, T. Do, P.R. Norton, G.M. Bancroft, M. Kasrai, T.W. Capelhart, Y.T. Cheng and T. Perry, *Tribol. Lett.* 15 (2003) 241.
- [32] A.J. Pidduck and G.C. Smith, *Wear* 212 (1997) 254.
- [33] O.L. Warren, J.F. Graham, P.R. Norton, J.E. Houston and T.A. Michalske, *Tribol. Lett.* 4 (1998) 189.
- [34] S. Bec and A. Tonck, *Nanometer scale mechanical properties of tribochemical films*, G. Dalmaz (Tribology Series: Lubricants and Lubrication, 1996) 30(Elsevier, Amsterdam, 1996) 173.
- [35] S. Bec, A. Tonck, J.M. Georges, R.C. Coy, J.C. Bell and G.W. Roper, *Proc. Roy. Soc. Lond. A* 455 (1999) 4181.
- [36] J.F. Graham, C. McCague and P.R. Norton, *Tribol. Lett.* 6 (1999) 149.
- [37] M.A. Nicholls, G.M. Bancroft, P.R. Norton, M. Kasrai, G. De Stasio, B.H. Frazer and L.M. Wiese, *Tribol. Lett.* 17 (2004) 245.
- [38] G.M. Bancroft, *Can. Chem. News* 44 (1992) 15.
- [39] B.X. Yang, F.H. Middleton, B.G. Olsson, G.M. Bancroft, J.M. Chen, T.K. Sham, K. Tan and D.J. Wallace, *Rev. Sci. Instrum.* 63 (1992) 1355.
- [40] M. Kasrai, Z. Yin, G.M. Bancroft and K. Tan, *J. Vacuum Sci. Technol. A* 11 (1993) 2694.
- [41] T. Tyliczszak, McMaster University, unpublished program.
- [42] T. Tyliczszak, BGAUSS—Multiline Fitting Program, Unpublished, Version 2.3, 1994.
- [43] M.A. Nicholls, P.R. Norton, G.M. Bancroft and M. Kasrai, *Wear* 257 (2004) 311.
- [44] B.H. Frazer, M. Girasole, L.M. Wiese, T. Franz and G. De Stasio, *Ultramicroscopy* 99 (2004) 87.
- [45] B.H. Frazer, B. Gilbert, B.R. Sonderegger and G. De Stasio, *Surf. Sci.* 537 (2003) 161.
- [46] M. Kasrai, W.N. Lennard, R.W. Brunner, G.M. Bancroft, J.A. Bardwell and K.H. Tan, *Appl. Surf. Sci.* 99 (1996) 303.
- [47] C. Jacobsen, S. Wirick, G. Flynn and C. Zimba, *J. Microsc.* 197 (2000) 173.
- [48] L.M. Croll, J.F. Britten, C. Morin, A.P. Hitchcock and H.D.H. Stoeber, *J. Synchrotron Radiat.* 10 (2000) 265.
- [49] W.C. Oliver and G.M. Pharr, *J. Mater. Res.* 7 (1992) 1564.
- [50] G.P. Huffman, S. Mitra, F.E. Huggins, N. Shah, S. Vaidya and F. Lu, *Energy Fuels* 5 (1991) 574.
- [51] M.L. Suominen-Fuller, L.R. Fernandez, G.R. Massoumi, W.N. Lennard and M. Kasrai, *Tribol. Lett.* 8 (2000) 187.
- [52] D.G.J. Sutherland, M. Kasrai, G.M. Bancroft, Z.F. Liu and K.H. Tan, *Phys. Rev. B* 48 (1993) 14989.
- [53] M. Fuller, Z. Yin, M. Kasrai, G.M. Bancroft, E.S. Yamaguchi, P.R. Ryason, P.A. Willermet and K.H. Tan, *Tribol. Int.* 30 (1997) 305.
- [54] Z. Zhang, M. Kasrai, G.M. Bancroft and E. Yamaguchi, *Tribology Lett.* 15 (2003) 377.
- [55] E. Yamaguchi, Z. Zhang, L.S. Kasten and G.M. Bancroft, *Tribol. Lett.* 15 (2003) 385.
- [56] P.A. Willermet, D.P. Dailey, R.O. Carter III, P.J. Schmitz, W. Zhu, J.C. Bell and D. Park, *Tribol. Int.* 28 (1995) 163.
- [57] B. Gilbert, R. Andres, P. Perfetti, G. Margaritondo, G. Rempfer and G. De Stasio, *Ultramicroscopy* 83 (2000) 129.
- [58] D. Shindo and T. Oikawa, *Energy Dispersive X-ray Spectroscopy. Analytical Electron Microscopy for Materials Science* (Springer-Verlag, Tokyo, 2002)Chapter 4.
- [59] A.V. Kulkarni and B. Bhushan, *Mater. Lett.* 29 (1996) 221.
- [60] G.M. Pharr and W.C. Oliver, *MRS Bull.* 17 (1992) 28.
- [61] P.J. Blau, *Friction, lubrication, and wear technology*, S. Henry (ASM Handbook, 1992) 18(The Materials Information Society, Materials Park, OH, 1992) 414.
- [62] H.A. Schaeffer, *Silica*, M.B. Bever (Encyclopedia of Materials Science and Engineering, 1986)(Pergamon Press, Oxford, England, 1986) 20.